Supporting Information: Characterizing aliphatic moieties in hydrocarbons with atomic force microscopy

Bruno Schuler,[1,*] Yunlong Zhang,[2,†] Sara Collazos,[3] Shadi Fatayer,[1] Gerhard Meyer,[1] Dolores Pérez,[3] Enrique Guitián,[3] Michael R. Harper,[2] J. Douglas Kushnerick,[2] Diego Peña,[3,‡] and Leo Gross[1]

[1] *IBM Research – Zurich, Säumerstrasse 4, 8803 Rüschlikon, Switzerland*

[2] *ExxonMobil Research and Engineering Company, Annandale NJ 08801, United States*

[3] *Centro de Investigación en Química Biolóxica e Materiais Moleculares (CIQUS) and Departamento de Química Orgánica, Universidade de Santiago de Compostela, Santiago de Compostela 15782 Spain*

(Dated: 6th December 2016)

Abstract

In this supplemental material additional scanning tunneling microscopy (STM) and atomic force microscopy (AFM) measurements as well as NMR, optical spectroscopy and gas chromatography (GC) characterization of the five model compounds are provided. For CPNP and CHNP the synthetic route is described.

CONTENTS

* bschuler@lbl.gov

† yunlong.zhang@exxonmobil.com

‡ diego.pena@usc.es

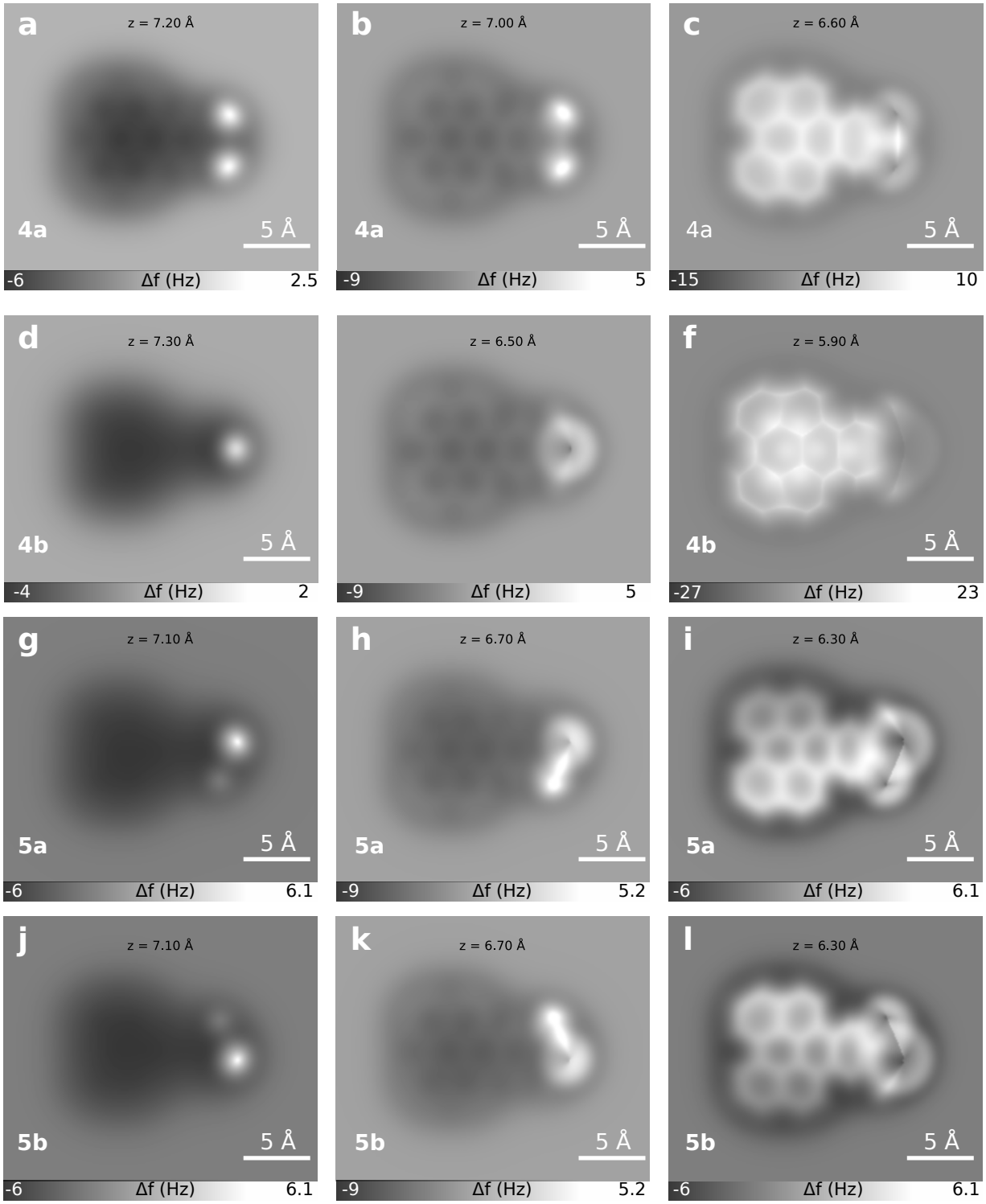

Figure S1. **AFM simulation.** Constant-height CO tip AFM simulations using the Probe Particle Model by Hapala et al. [1, 2].

I. STM/AFM SUPPORTING EXPERIMENTS

A. AFM simulation for CPNP and CHNP

We employed the Probe Particle Model by Hapala et al. [1, 2] to simulate constant-height AFM images of the molecules CPNP, **4**, and CHNP, **5**, in their different respective adsorption geometries **4a**, **4b**, **5a** and **5b**. For the calculations we used standard parameters with a CO tip, i.e., a lateral spring constant of the tip of 0.25 N/m as supported by experiment [3]. For the molecular structures we used the relaxed geometries of the free molecules using FHI-AIMS [4]. The imaging plane was parallel to the molecular plane at distance z from the perylene core of the molecules. Geometries **4a** and **4b** were obtained by scanning the same molecule from either side. We chose differences of tip heights z between the images matching the relative height offsets in the experimental images shown the main text. Therefore, images Figs. S1a-c can be compared to Figs. 5b-d, respectively; Figs. S1d-f can be compared to Figs. 5f-h, respectively; and Figs. S1g-h can be compared to Figs. 6b-d, respectively. Note that in the simulations there is no substrate. But the planar substrate can be expected to yield only a constant background in constant-height AFM images. Therefore, the absolute Δf values will differ between experiment and theory, but the relative contrast can be compared. We note that for all molecules and all geometries we observe a relatively good agreement between experiment and simulation for the large and medium tip heights (the left and the center column in Fig. S1). This agreement corroborates that our assignment of the different molecular adsorption geometries. However, for the smallest tip heights (right column in Fig. S1), the contrast above the aliphatic moieties of the molecule shows significant deviations when comparing experiment and simulations. This indicates the difficulties of simulating AFM images above non-planar groups at small tip heights, at which tip relaxations play an important role. It is also possible that at the small tip heights the adsorption geometry of the CPNP and CHNP molecules is altered by interaction with the tip. This effect is not captured in the simulations, which take only relaxations of the tip into account. These deviations at small tip heights illustrate the importance of establishing experimental AFM data for fingerprinting of molecular moieties for their identification in *a priori* unknown samples.

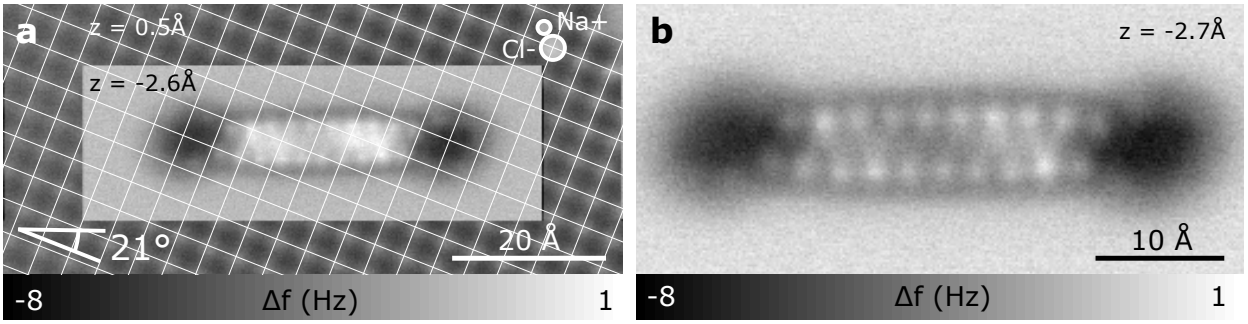

Figure S2. **BPI adsorption site on NaCl. a** CO tip AFM image of BPI on NaCl using different scan heights on the substrate and close to the molecule [5]. Grid intersections indicate Cl positions. **b** CO tip AFM image of the same molecule at a slightly larger distance to highlight the contrast modulations among methylene groups.

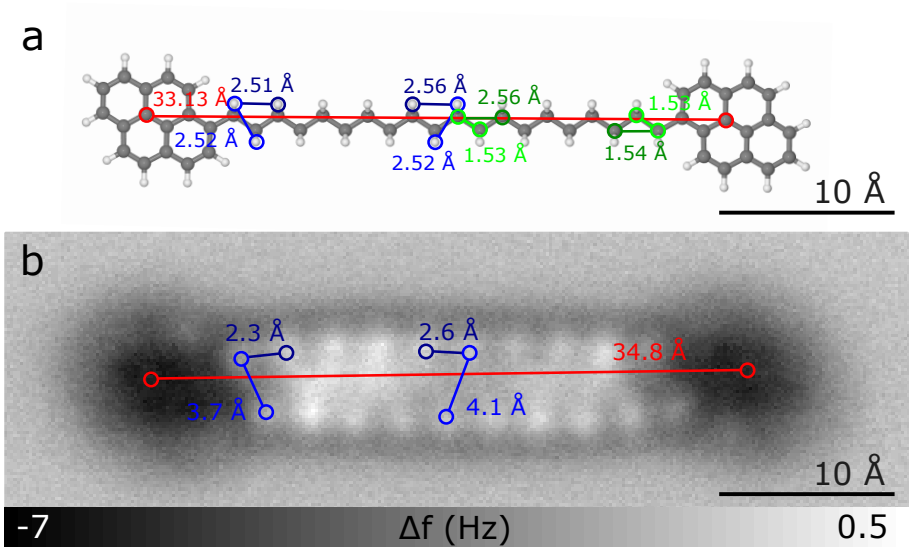

Figure S3. **BPI length comparison. a** Density functional theory calculated geometry of the free BPI molecule. **b** CO tip AFM measurmeent of BPI on NaCl. The lines in a and b indicate distances between carbon pairs (red, green) or H pairs (blue).

B. BPI adsorption site and apparent size

BPI's long axis adsorbs 21° with respect to the polar NaCl direction (see Fig. S2a). We attribute the faint AFM contrast modulations along the alkyl chain (see Fig. S2b) to adsorption height differences in response to the substrate registry.

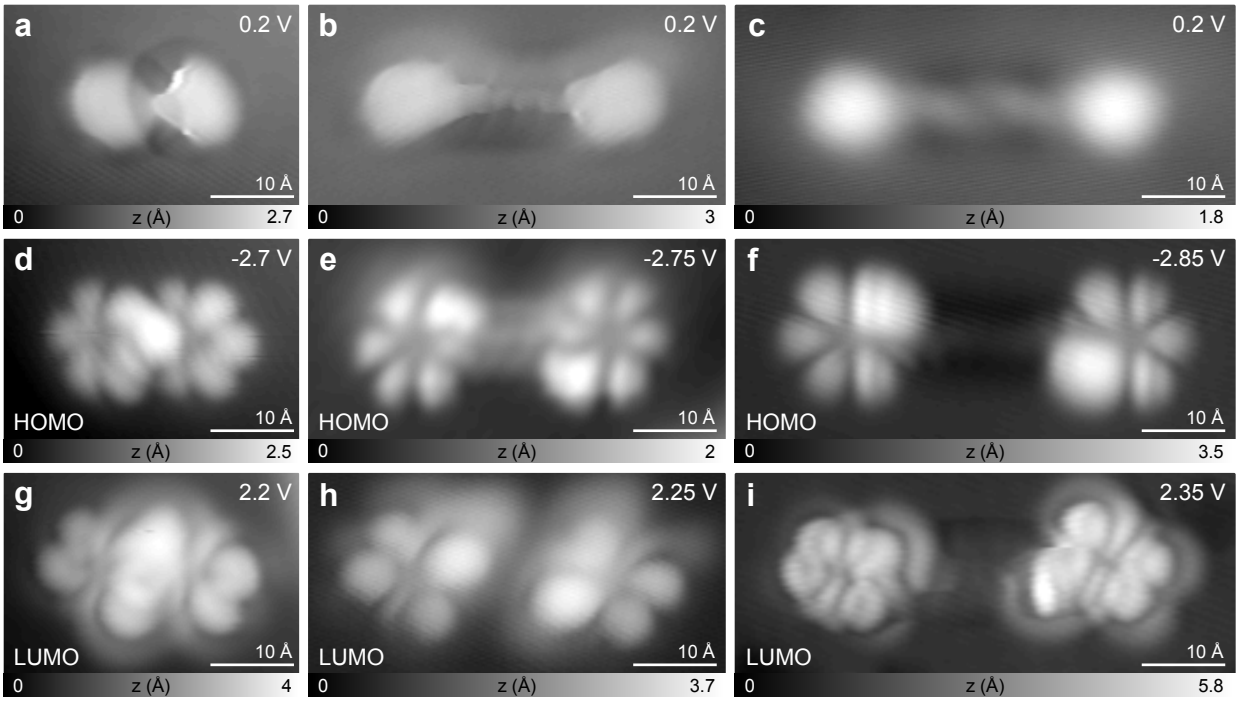

Figure S4. **STM orbital imaging of BPE, BPD and BPI. a-c** In-gap STM images of BPE, BPD and BPI on NaCl(2ML)/Cu(111), respectively. **d-f** STM image of the HOMO resonance of the same molecules. **g-i** STM image of the LUMO resonance of the same molecules.

In Fig. S3 the calculated (for the free molecule) and experimental distances of intramolecular features in BPI are compared. The overall length of the molecule agrees within the measurement accuracy to the calculated model. Also the H–H distances between adjacent methylene groups along the molecule's long axis (Fig. S3b dark blue) are in good agreement with the calculated values. Along the short axis (Fig. S3b light blue), however, the apparent H–H distances are significantly enlarged by about 50-60% as compared to the calculated values. One can also observe an apparent widening of the chain when going from the pyrene terminus towards the chain center. Both the enlarged appearance and widening of the chain perpendicular to its long axis are attributed to CO tip bending effects [1, 6, 7].

C. Molecular orbital imaging

For the three dipyrene molecules (BPE, BPD and BPI) the frontier molecular orbitals could be measured by STM orbital imaging [8] as shown in Fig. S4. Both the highest occupied (HOMO) and lowest unoccupied molecular orbital (LUMO) are localized on the aromatic

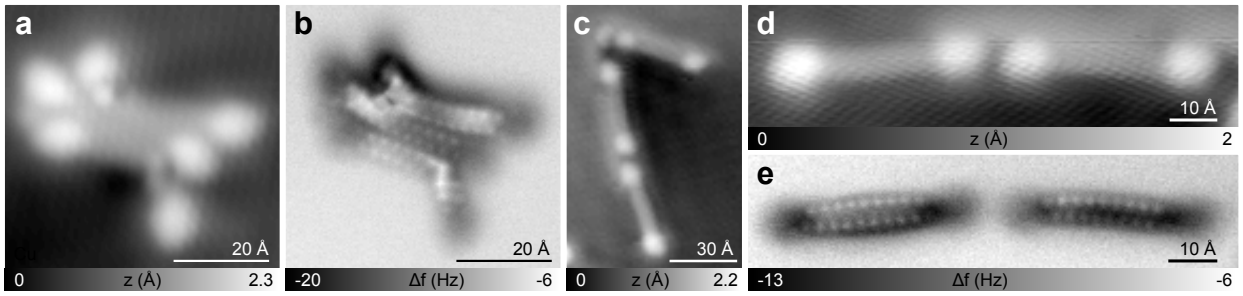

Figure S5. **BPI post annealing to room temperature. a,b** STM (a) and AFM (b) image of three BPI molecules in a conglomerate. **c** STM image of three BPI molecules adsorbed along a Cu(111) screw dislocation. **d,e** STM (d) and AFM (e) image of two BPI molecules adsorbed along a Cu(111) step edge.

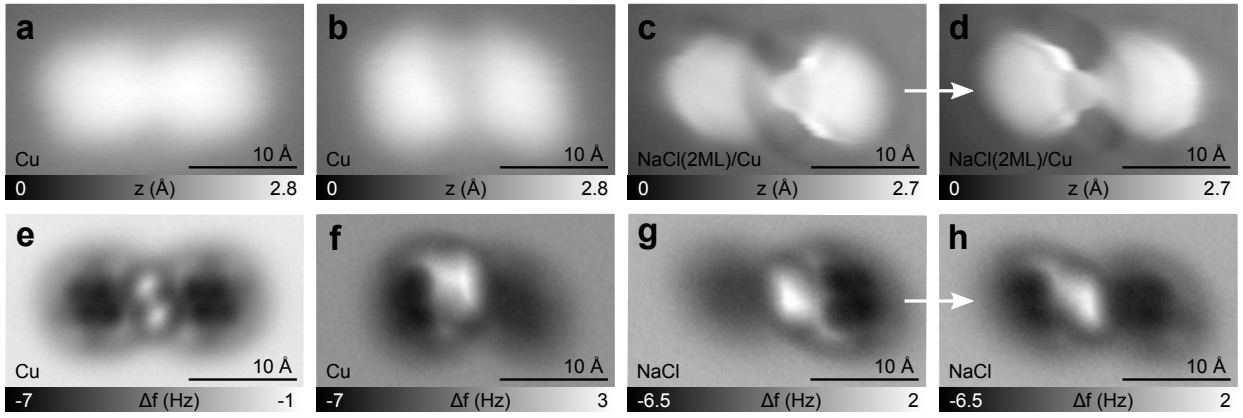

Figure S6. **BPE conformations**. **a,e** STM (a) and AFM (e) image of BPE in the trans, flat conformation on Cu. **b,f** STM (b) and AFM (f) image of BPE in the cis, up-down conformation on Cu. **c,g** STM (c) and AFM (g) image of BPE in the trans, down-up conformation on NaCl. **d,h** STM (d) and AFM (h) image of BPE in the trans, up-down conformation on NaCl.

pyrene moieties and the aliphatic chain linker does not contribute, as expected. The good agreement with the calculated molecular orbitals (not shown here) for these molecules is further proof of the intactness of these molecules. For CPNP and CHNP, the molecular orbitals could not be measured because inelastic excitations of the molecules triggered their dislocation.

D. Conformation change by annealing or tip-induced

The linear and cyclic aliphatic groups can adopt multiple adsorption geometries as described in the main paper and illustrated in Fig. 2 for BPI and Figs. 5 and 6 for CPNP and CHNP, respectively. The small difference in adsorption energies between the different conformations allows the molecule to stabilize different adsorption geometries on the surface when evaporated on the cold sample. For longer linear aliphatic chains, however, the straight flat geometry is preferred, which is adopted after annealing the sample to room temperature. As seen in Fig. S5, the BPI molecules align all straight and are pinned to defects, step edges or small aggregates. Sometimes a single twist remains in the chain when the pyrene units adsorb initially in the trans conformation (e.g. the bottom molecule in Fig. S5b).

Inelastic excitations of the molecule by tunneling electrons on both Cu and NaCl substrate preferentially straighten longer linear aliphatic chains as well. This is illustrated in Figs. 2h-k of the main manuscript. For the small C_2H_4 linker in BPE the flat geometry is only observed on Cu along with three other adsorption geometries, i.e. the two pyrenes in cis or trans where the zig-zag structure of the alkyl chain is either oriented parallel or vertical to the surface. On NaCl, only the vertical geometry was found, being either up-down or down-up (see Fig. S6). One could also switch repeatedly between these two conformations. The characteristic tip-induced conformational changes provide another fingerprint of the aliphatic moieties.

E. Tip-induced dehydrogenation

On the Cu surface it was possible to cleave hydrogen atoms from all five molecules by voltage pulses applied to the tip, indicating a tip-induced on-surface oxidation process [9]. Cleaving 4 H from the CHNP molecule, which can be done sequentially, leads to a full aromatization of the molecules (see Fig. 6h) as schematically shown in Fig. S7. This provides further evidence that CHNP could be deposited intact without loosing hydrogen during the evaporation step.

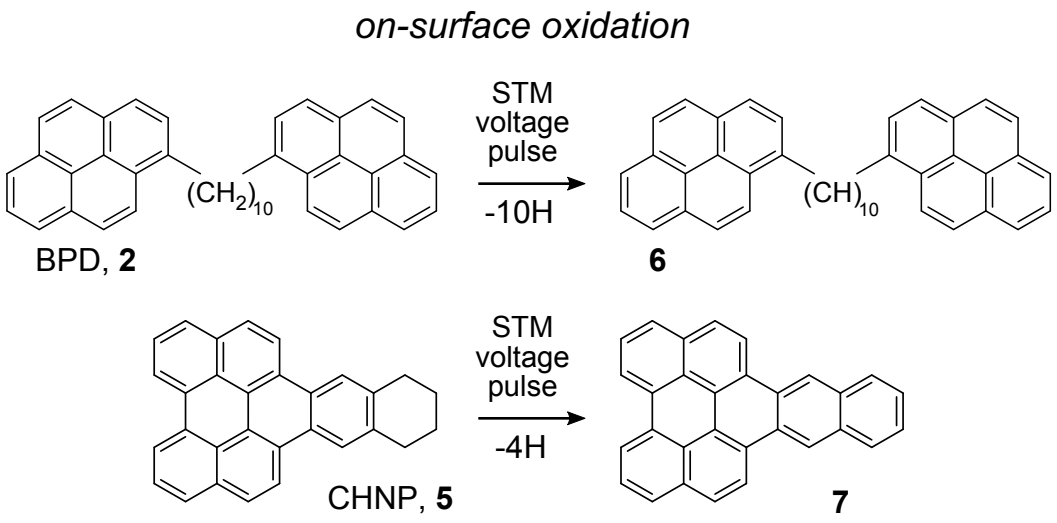

Figure S7. **On-surface oxidation process.** Tip-induced dehydrogenation on Cu.

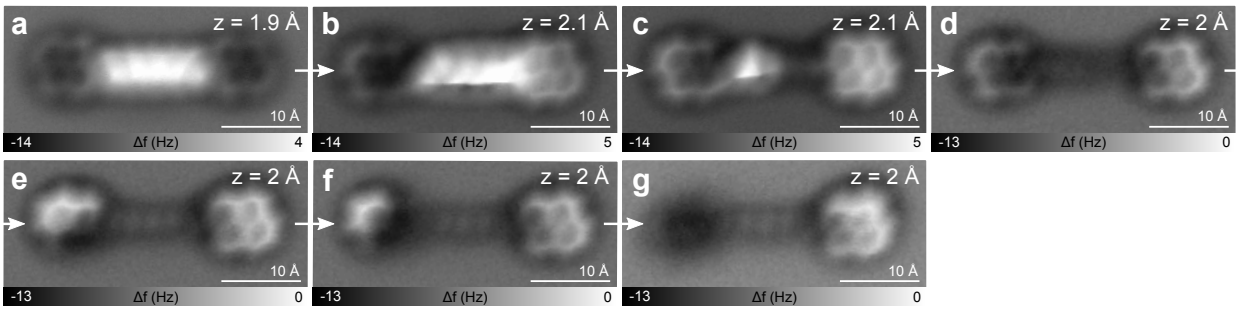

Figure S8. **BPD sequential dehydrogenation. a-g** AFM images of BPD on Cu after tip-induced dehydrogenation by voltage pulses. Sometimes several voltage pulses were applied between consecutive images. At a voltage of 3.5 V, H from the alkyl chain is abstracted (a-d). At higher voltages around 3.8 V, H from the aromatic pyrene ring can be removed (d-g).

For BPD we could dissociate H from the alkyl chain with bias pulses of about 3.5 V until each C atom has lost one hydrogen as illustrated in Fig. S7. A sequence of products after H dissociation is shown in Figs. S8a-d. Note that not all intermediate steps are shown here. With slightly higher voltage pulses of about 3.8 V, the hydrogens from the pyrene could be cleaved as well until the entire pyrene moiety was dehydrogenated (Figs. S8e-g). The hydrogen abstraction leads to a considerable increase of the molecule–substrate interaction such that the respective moiety adsorbs more closely to the Cu surface [5]. Strikingly, the tip pulse necessary to cleave the C–H bonds of the aliphatic moieties was approximately the same for all five molecules suggesting a dominant role of the Cu substrate in this process.

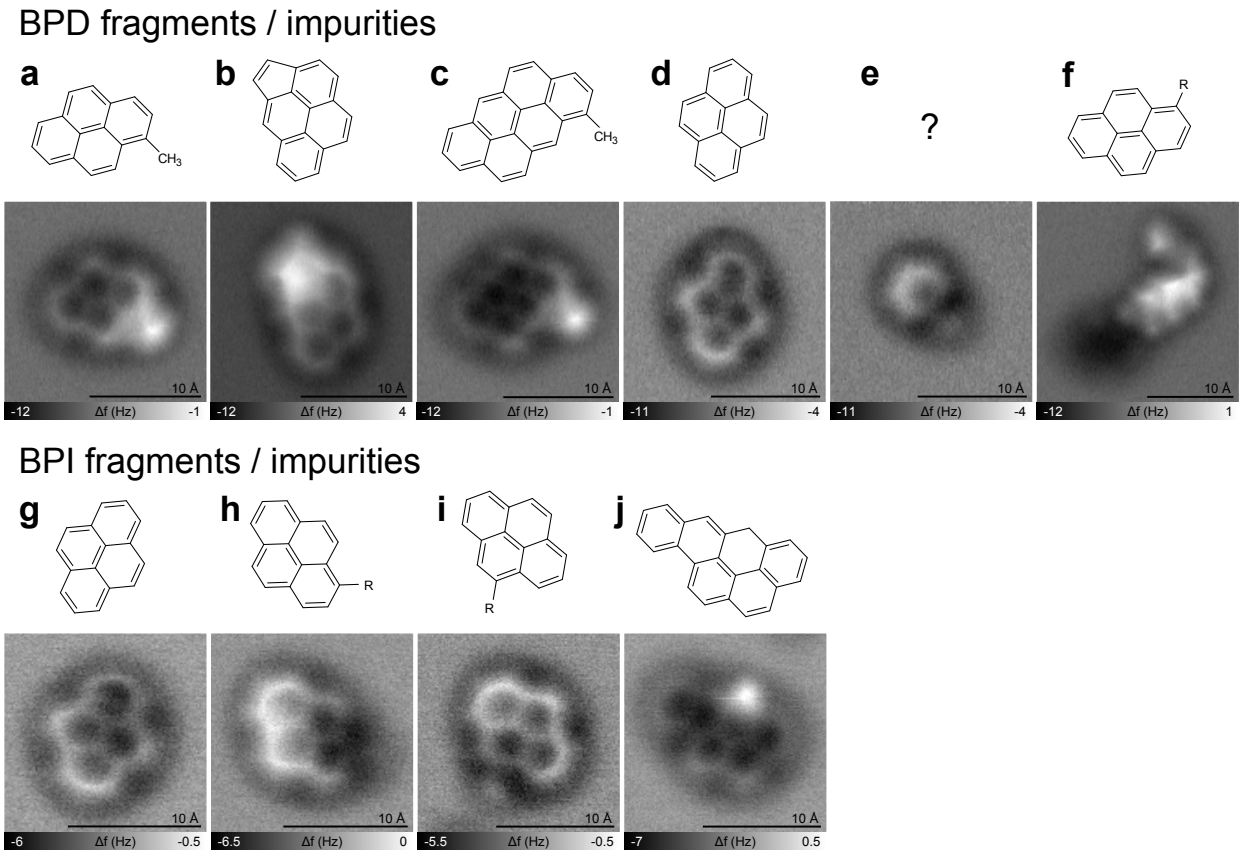

Figure S9. **Fragments or impurities on BPD and BPI samples. a-j** CO tip AFM measurements of fragments or impurities of BPD and BPI found on the surface and their assigned chemical structure. R denotes an unknown rest group.

F. Additional molecules on the BPD and BPI samples

As mentioned in the main manuscript, although the majority of the molecules could be deposited intact, we observed some additional molecules in the BPD and BPI sample. AFM measurements of some of these molecules are shown in Fig. S9 along with their structural assignments.

From the AFM measurements itself it is not directly possible to distinguish impurities of the initial sample from fragments formed during sublimation. From GC and boiling point analysis one can estimate the presence of about 4 wt% of impurities in the BPD and BPI samples. Furthermore, GC/LC-MS and NMR data show that the impurity concentration has to be allocated to a broad spectrum of species as they were hidden in the baseline.

The AFM data presented in Fig. S9 supports this interpretation. The size of the additional molecules measured by AFM suggests that the impurity concentration of the source material in number of molecules is on the order of 8 %, in agreement with the value derived from AFM measurements. A few molecules detected (Figs. S9f,h,i), however, could tentatively also be allocated to fragments of the main compound that are potentially formed during evaporation. Since these molecules were found on Cu, no orbital imaging was possible to verify this hypothesis. Importantly, the vast majority of the molecules adsorb intact, providing clear evidence that fast thermal evaporation is a suitable method to apply the model molecules studied here on the surface.

II. BPE, BPD AND BPI MOLECULES SYNTHESIS AND ADDITIONAL CHARACTERIZATION

A. General methods

BPD was obtained from Setareh Biotech, LLC (OR, USA), and BPE and BPI from Tyger Scientific, Inc. (NJ, USA). The synthesis of BPD, BPE, and BPI has been described previously [10–13]. High temperature gas chromatography (simulated distillation approximately similar to American Standard Testing Materials-ASTM D7169 test method) with a flame ionization detector was used to determine the purity and boiling point of each sample [11]. The boiling point calibration was based on a mixture of pure n-paraffins and a hydrocarbon polywax. The measured purity (obtained by manual integration of the gas chromatographic signal shown in Figs. S15-S16 and assumed an equal signal response for the impurities and the major compounds) and boiling point are: BPD (99.5%, 592 °C), BPE (97.3%, 555 °C), and BPI (96.3%, 638 °C). ^{1}H NMR and ^{13}C NMR spectra were recorded at 400 MHz and 100 MHz (Bruker Ultrashield 400 NMR spectrometer). UV-Vis absorption was measured with a JASCO V-7200 spectrophotometer.

B. Experimental details and spectroscopic data

Spectroscopic data for BPE, **1**:
^{1}H NMR (298 K, 400 MHz, $CDCl_3$) δ: 8.42 (d, J = 8.0 Hz, 2H), 8.19-8.21 (m, 4H), 8.15 (d, J = 8.0 Hz, 2H), 8.00-8.09 (m, 8H), 7.83 (d, J = 8.0 Hz, 2H), 3.90 (s, 4H) ppm. ^{13}C NMR (298 K, 100 MHz, $CDCl_3$) δ: 135.97, 131.47, 130.94, 130.02, 128.71, 127.58, 127.52, 127.35, 126.73, 125.88, 125.16, 125.09, 124.99, 124.89, 124.81, 123.22, 35.65 ppm.

Spectroscopic data for BPD, **2**:
^{1}H NMR (298 K, 400 MHz, $CDCl_3$) δ 8.28 (d, J = 9.2 Hz, 2H), 8.14-8.16 (d, J = 8.0 Hz, 4H), 8.07-8.11 (m, 4H), 8.00-8.04 (m, 4H), 7.95-7.99 (m, 2H), 7.86 (d, J = 7.6 Hz, 2H), 3.32 (t, J = 8.0 Hz, 4H), 1.81-1.88 (m, 4H), 1.42-1.49 (m, 4H), 1.31-1.42 (m, 8H) ppm. ^{13}C NMR (298 K, 100 MHz, $CDCl_3$) δ: 137.34, 131.43, 130.92, 129.65, 128.58, 127.52, 127.23, 127.05, 126.44, 126.27, 125.72, 125.06, 125.05, 124.74, 124.58, 123.52, 33.60, 31.92, 29.58,

29.78, 29.58, 29.55 ppm.

Spectroscopic data for BPI, **3**:
^{1}H NMR (298 K, 400 MHz, $CDCl_3$) δ: 8.28 (d, J = 8.0 Hz, 2H), 8.14-8.16 (m, 4H), 8.08-8.11 (m, 4H), 7.96-8.04 (m, 6H), 7.86 (d, J = 8.0 Hz, 2H), 3.33 (t, J = 8.0 Hz, 4H), 1.83-1.87 (m, 4H), 1.46-1.53 (m, 4H), 1.35-1.39 (m, 4H), 1.25-1.26 (m, 24H) ppm. ^{13}C NMR (298 K, 100MHz, $CDCl_3$) δ: 137.38, 131.44, 130.94, 129.66, 128.59, 127.52, 127.23, 127.05, 126.44, 125.73, 125.07, 124.75, 124.58, 123.53, 33.62, 31.96, 29.83, 29.66, 29.63, 29.58 ppm.

^{1}H and ^{13}C NMR spectra of BPE, BPD and BPI are shown in Figs. S10-S12, respectively. UV-Vis absorption spectra are provided in Fig. S13 and experimental high temperature GC data is shown in Figs. S14-S16.

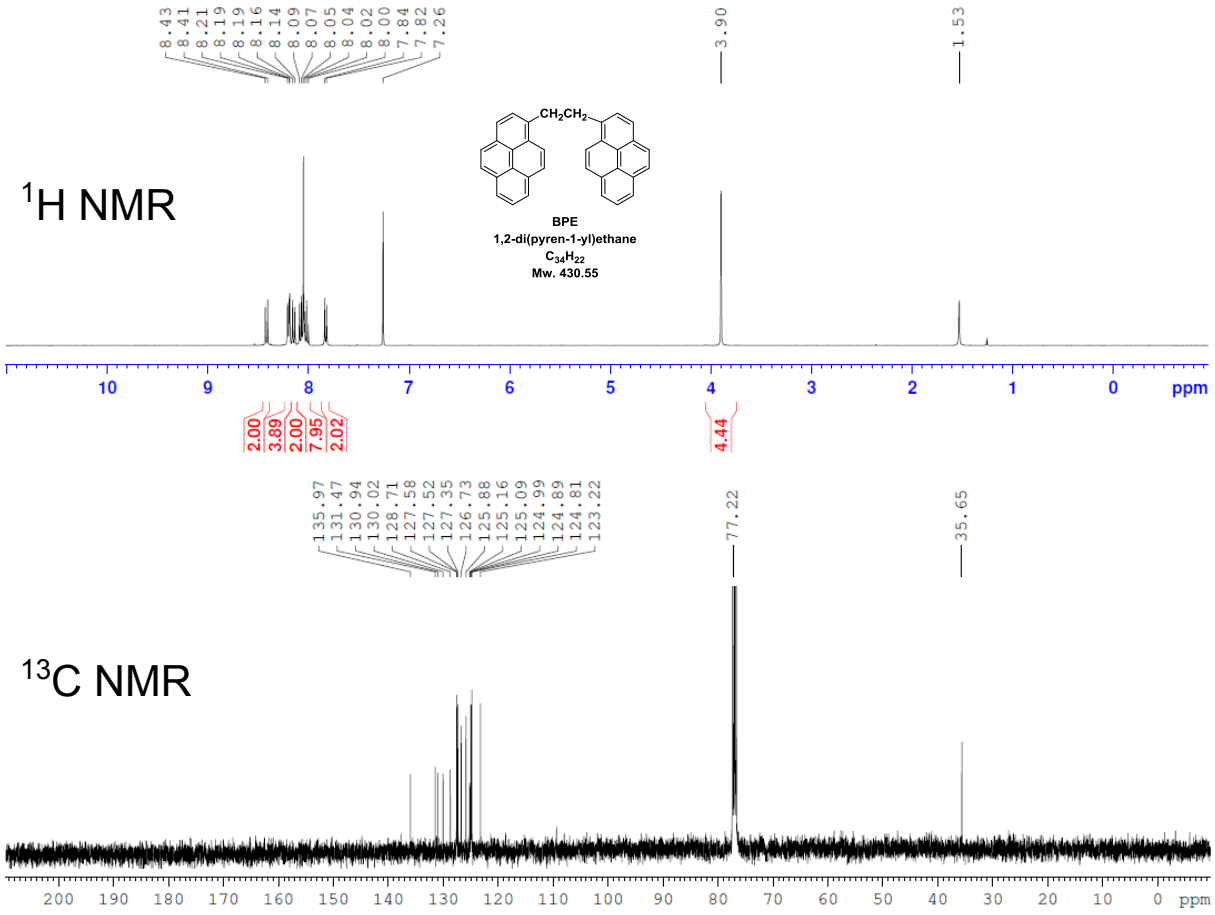

Figure S10. ^{1}H and ^{13}C NMR spectra of BPE, **1**.

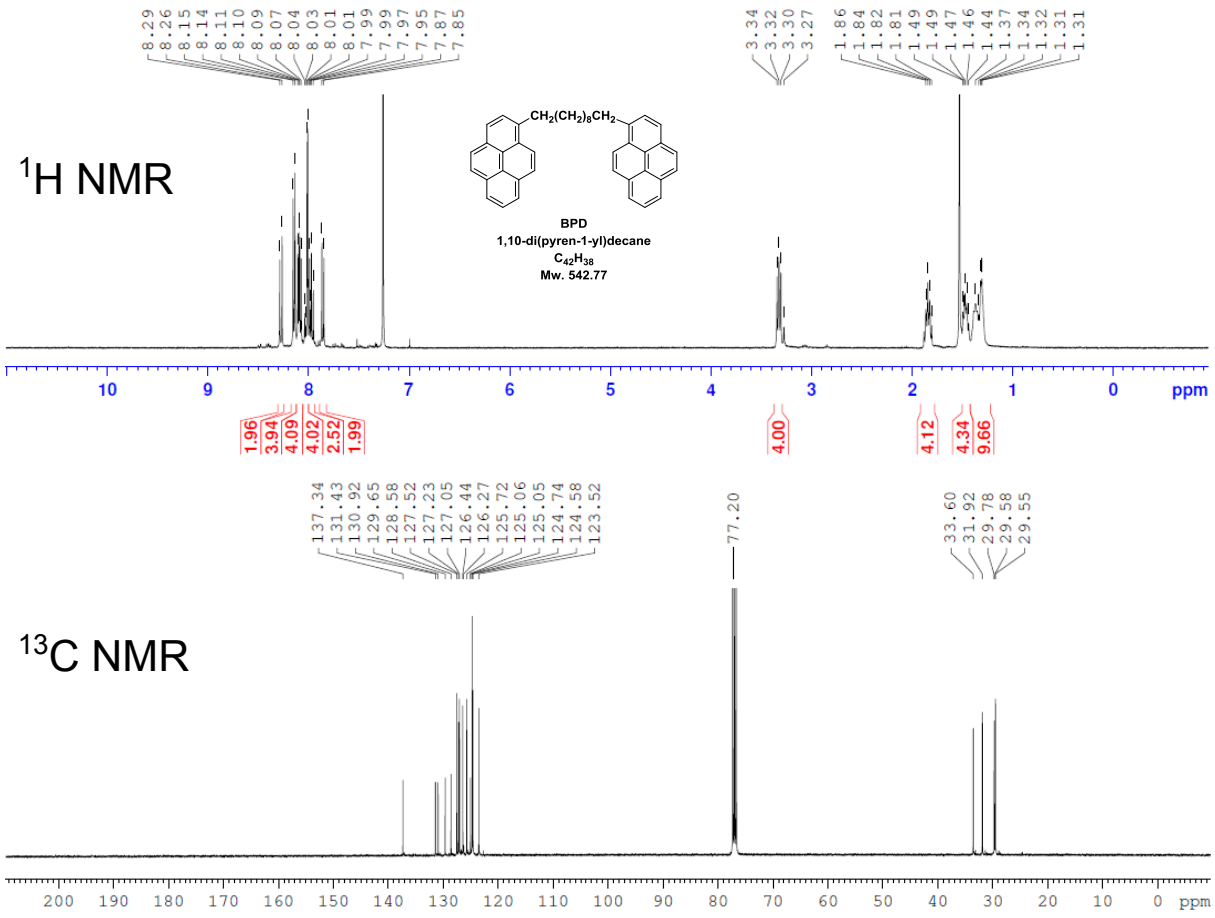

Figure S11. ^{1}H and ^{13}C NMR spectra of BPD, **2**.

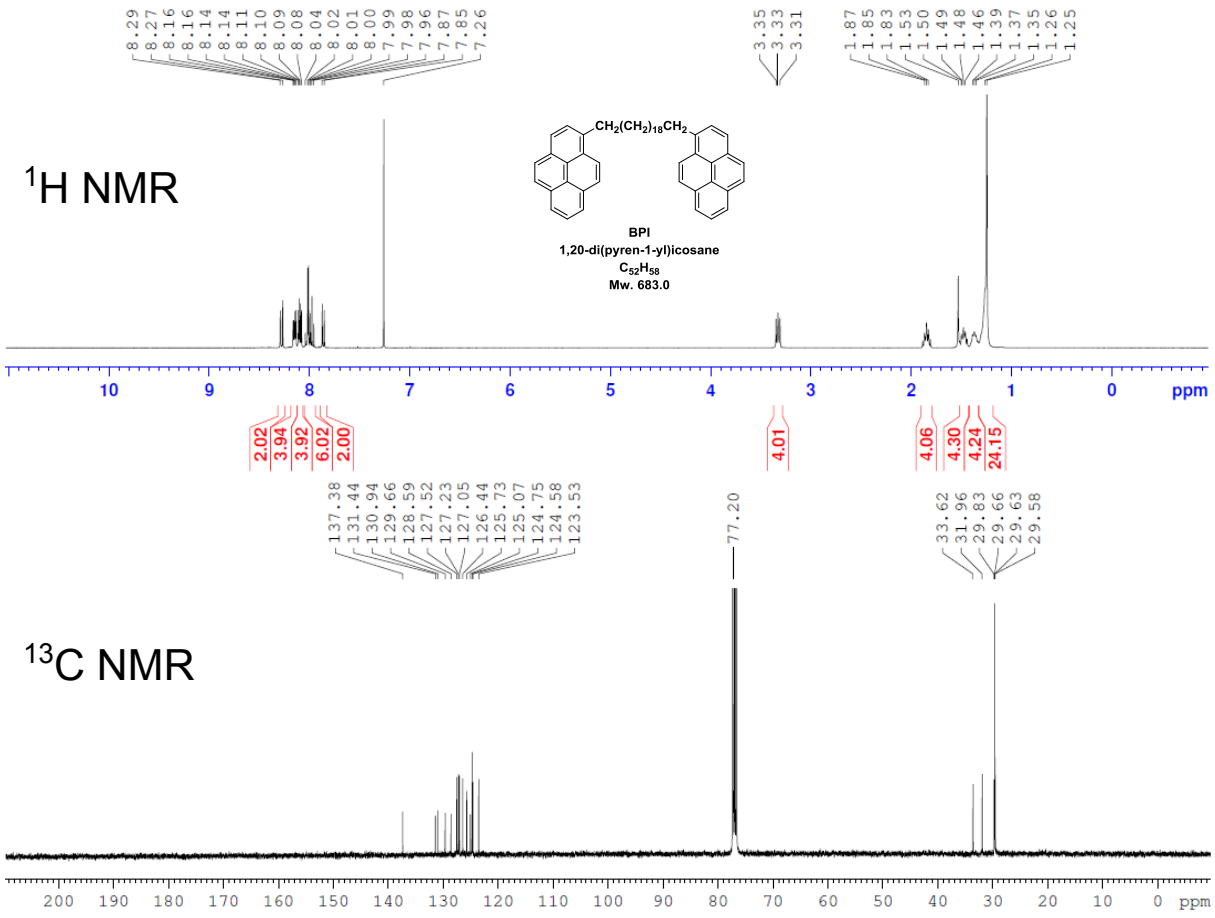

Figure S12. ^{1}H and ^{13}C NMR spectra of BPI, **3**.

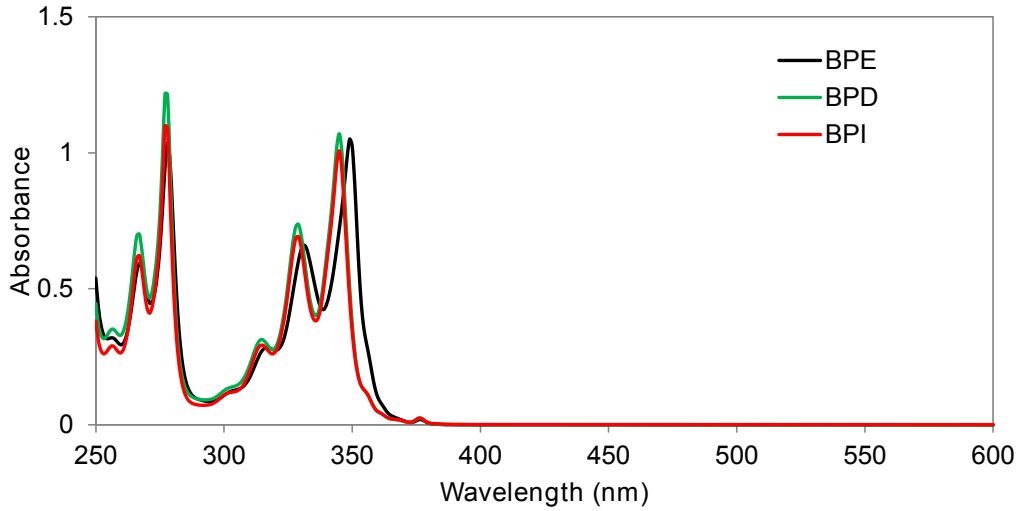

Figure S13. UV-Vis absorption spectrum of BPE (**1**), BPD (**2**), and BPI (**3**) in CH_2Cl_2.

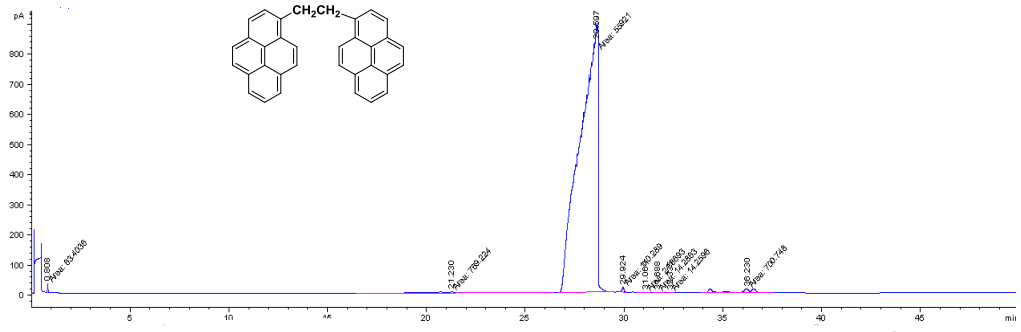

Figure S14. High temperature GC chromatogram for BPE, **1**.

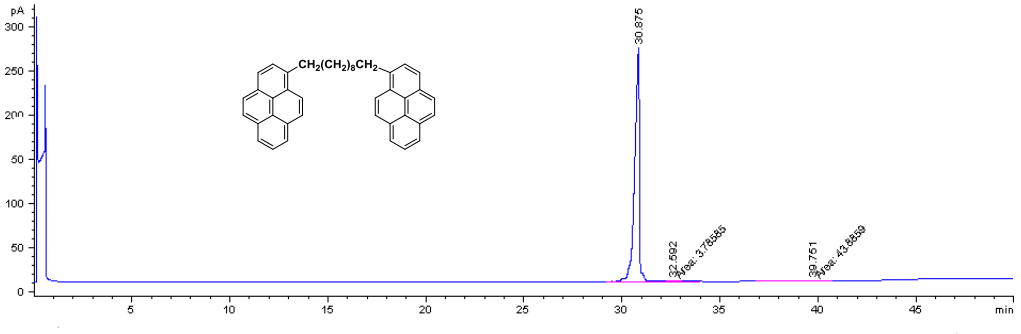

Figure S15. High temperature GC chromatogram of BPD, **2**.

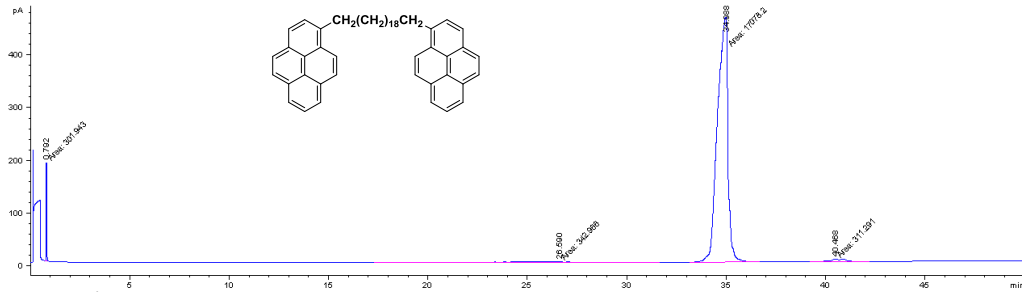

Figure S16. High temperature GC chromatogram for BPI, **3**.

III. CPNP AND CHNP MOLECULES SYNTHESIS AND ADDITIONAL CHARACTERIZATION

A. General methods

All reactions were carried out under argon using oven-dried glassware. TLC was performed on Merck silica gel 60 F_{254}; chromatograms were visualized with UV light (254 and 360 nm). Flash column chromatography was performed on Merck silica gel 60 (ASTM 230-400 mesh). ^{1}H and ^{13}C NMR spectra were recorded at 300 and 75 MHz (Varian Mercury-300 instrument) or 500 and 125 MHz (Bruker DPX-500 instrument), respectively. Low-resolution electron impact mass spectra were determined at 70 eV on HP-5988A instrument. High-resolution mass spectra (HRMS) were obtained on a Micromass Autospec spectrometer. UV/Vis spectra were obtained on a Varian Cary 100 Bio or a Jasco V-530 spectrophotometers.

Commercial reagents were purchased from ABCR GmbH, Aldrich Chemical Co., or Strem Chemicals Inc., and were used without further purification. *n*-BuLi was used in hexane solution (2.5 M). Anhydrous solvents were purified on a MBRAUN SPS 800 instrument. Triflate **8** (Fig. S17) was prepared following a published procedure [14]. Similarly, triflate **9** was synthesized as described in section III B 1.

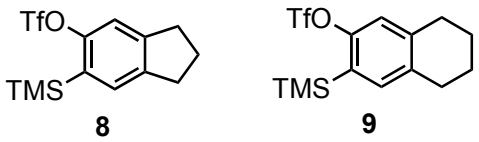

Figure S17. Triflates **8** and **9** used as aryne precursors.

B. Experimental details and spectroscopic data

1. *Synthesis of triflate **9***

A solution of bromine (554 μL, 10.8 mmol) in AcOH (11 mL) was added dropwise to a solution of 5,6,7,8-tetrahydro-2-naphthol (**10**, 2.0 g, 13.5 mmol) in a mixture of AcOH (45

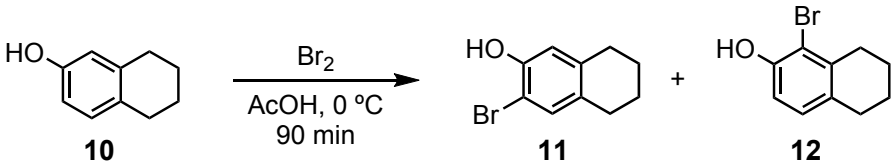

Figure S18. Synthesis of compound **11**.

mL) and CH_2Cl_2 (9.3 mL) at 0 °C. The mixture was stirred at this temperature for 90 min. Then, an aqueous solution of $Na_2S_2O_3$ (10%, 20 mL) was added, and the resulting mixture was extracted with CH_2Cl_2 (3 x 20 mL). The combined organic layers were dried over Na_2SO_4, filtered and concentrated under reduced pressure. The residue was purified by column chromatography (SiO_2; 5% Et_2O in hexane) to obtain compound **11** (420 mg, 14%) and **12** (1.42 g, 46%) as white solids [15].

Spectroscopic data for compound **11**

^{1}H NMR (298 K, 300 MHz, $CDCl_3$): δ 7.15 (s, 1H), 6.72 (s, 1H), 5.25 (s, OH), 2.71 – 2.64 (m, 4H), 1.78 – 1.72 (m, 4H) ppm. ^{13}C NMR (298 K, 75 MHz, $CDCl_3$), δ: 149.94 (C), 138.69 (C), 132.05 (CH), 131.17 (C), 116.10 (CH), 107.20 (C), 29.19 (CH_2), 28.42 (CH_2), 23.10 (CH_2), 22.90 (CH_2) ppm. MS (EI), m/z (%): 226.0 (100). HRMS (EI) for $C_{10}H_{11}OBr$, calculated: 225.9993, found: 225.9998.

Spectroscopic data for compound **12**

^{1}H NMR (298 K, 300 MHz, $CDCl_3$), δ: 6.95 (d, J = 8.3 Hz, 1H), 6.82 (d, J = 8.3 Hz, 1H), 5.48 (s, OH), 2.76 – 2.68 (m, 4H), 1.88 – 1.69 (m, 4H) ppm. ^{13}C NMR (298 K, 75 MHz, $CDCl_3$), δ: 150.27 (C), 136.82 (C), 131.27 (C), 129.37 (CH), 113.68 (C), 113.03 (CH), 30.55 (CH_2), 29.33 (CH_2), 23.19 (CH_2), 22.72 (CH_2) ppm. MS (EI), m/z (%): 226.0 (100). HRMS (EI) for $C_{10}H_{11}OBr$, calculated: 225.9993, found: 225.9997.

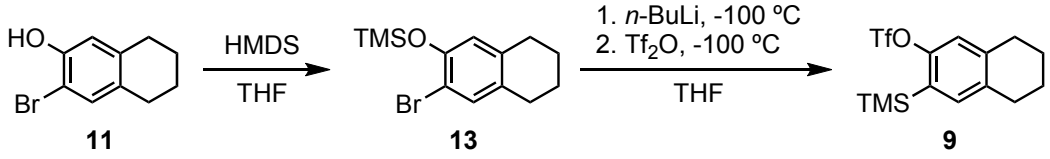

Figure S19. Synthesis of triflate **9**.

A mixture of 3-bromo-5,6,7,8-tetrahydro-2-naphthol (**11**, 400 mg, 1.77 mmol) and hexamethyldisilazane (HMDS, 806 μL, 3.72 mmol) in THF (800 μL) was refluxed for 90 min. Then, the solvent was evaporated under reduced pressure and the residue was subjected to vacuum to remove unreacted HMDS. The crude compound **13** was dissolved in THF (12.6 mL), the solution was cooled to −100 °C, and *n*-BuLi (hexane solution, 2.5 M, 780 μL, 1.95 mmol) was added dropwise. Stirring was kept up while the temperature reached −80 °C. The mixture was again cooled to −100 °C, Tf_2O (327 μL, 1.95 mmol) was added dropwise, and stirring was again kept up while the temperature returned to −80 °C. Then, a saturated aqueous solution of $NaHCO_3$ (20 mL) was added, and the resulting mixture was extracted with Et_2O (3 x 20 mL). The combined organic layers were dried over Na_2SO_4, filtered and concentrated under reduced pressure. The residue was purified by column chromatography (SiO_2; 5% Et_2O in hexane) to obtain triflate **9** (306 mg, 49%) as a colorless oil.

Spectroscopic data for compound **13**

^{1}H NMR (298 K, 500 MHz, $CDCl_3$), δ: 7.20 (s, 1H), 6.57 (s, 1H), 2.69 – 2.63 (m, 4H), 1.77 – 1.72 (m, 4H), 0.29 (s, 9H) ppm. ^{13}C NMR (298 K, 125 MHz, $CDCl_3$), δ: 149.87 (C), 137.45 (C), 133.26 (CH), 131.91 (C), 120.96 (CH), 112.22 (C), 29.27 (CH_2), 28.52 (CH_2), 23.20 (CH_2), 23.03 (CH_2), 0.55 (3 CH_3) ppm.

Spectroscopic data for compound **9**

^{1}H NMR (298 K, 300 MHz, $CDCl_3$), δ: 7.17 (s, 1H), 7.01 (s, 1H), 2.79 – 2.69 (m, 4H), 1.81 – 1.73 (m, 4H), 0.33 (s, 9H) ppm. ^{13}C NMR (298 K, 75 MHz, $CDCl_3$), δ: 153.13 (C), 141.20 (C), 137.10 (CH), 136.83 (C), 129.11 (C), 119.94 (CH), 118.75 (q, J = 320.3 Hz, CF_3), 29.56 (CH_2), 28.89 (CH_2), 22.99 (CH_2), 22.64 (CH_2), -0.75 (3 CH_3) ppm. MS (EI), m/z (%): 352.0 (6). HRMS (EI) for $C_{14}H_{19}F_3O_3SSi$, calculated: 352.0776, found: 352.0772.

^{1}H and ^{13}C NMR spectra of compounds **9** and **11-13** are shown in Figs. S23-S26.

2. Synthesis of 11,12-dihydro-10H-cyclopenta[6,7]naphtho[1,2,3,4-ghi]perylene (CPNP, 4)

A mixture of perylene (**14**, 50 mg, 0.198 mmol), triflate **8** (134 mg, 0.396 mmol) and CsF (181 mg, 1.19 mmol) in THF/CH_3CN (1:1, 8 mL) was stirred at 60 °C for 16 h. The

resulting suspension was filtered to give a residue, which was subsequently washed with H_2O (2 x 2 mL), CH_3OH (2 x 2 mL) and Et_2O (4 x 2 mL) to afford compound **4** (45.2 mg, 63%) as a yellow solid. Mp: 234 °C (dec).

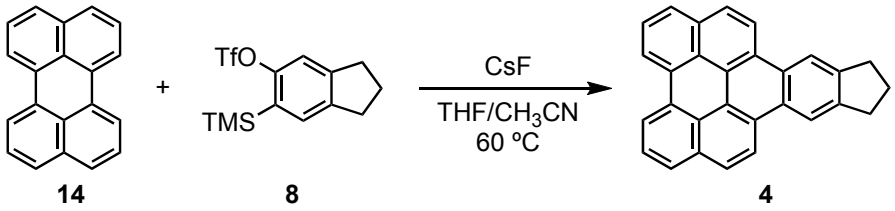

Figure S20. Synthesis of CPNP, **4**.

Spectroscopic data for compound **4**

^{1}H NMR (323 K, 500 MHz, $CDCl_3$), δ: 8.87 (d, J = 9.1 Hz, 2H), 8.82 (d, J = 7.1 Hz, 2H), 8.83 (s, 2H), 8.11 (d, J = 9.3 Hz, 2H), 8.09 (d, J = 8.5 Hz, 2H), 7.88 (t, J = 7.7 Hz, 2H), 3.30 (t, J = 7.3 Hz, 4H), 2.31 (q, J = 7.2 Hz, 2H) ppm. ^{13}C NMR (323 K, 125 MHz, $CDCl_3$), δ: 144.11 (2C), 132.56 (2C), 130.98 (2C), 127.85 (2C), 127.57 (2CH), 126.93 (2CH), 126.93 (2C), 126.58 (2C), 126.21 (2CH), 123.16 (2C), 122.37 (2CH), 120.61 (2CH), 118.39 (2CH), 33.41 (2 CH_2), 26.34 (CH_2) ppm. MS (EI), m/z (%): 366 (M^+, 100). MS (EI), m/z (%): 366 (M^+, 100). HRMS (EI), $C_{29}H_{18}$, calculated: 366.1409, found: 366.1409.

For experimental UV/Vis fluorescence spectra of compound **4** see Fig. S22a. ^{1}H and ^{13}C NMR spectra of compounds **4** are shown in Fig. S27.

*3. Synthesis of 10,11,12,13-tetrahydroanthra[1,2,3,4-ghi]perylene (CHNP, **5**)*

A mixture of perylene (**14**, 50 mg, 0.198 mmol), triflate **9** (70 mg, 0.198 mmol) and CsF (90 mg, 0.594 mmol) in THF/CH_3CN (1:1, 8 mL) was stirred at 60 °C for 16 h. The resulting suspension was filtered to give a residue, which was subsequently washed with H_2O (2 x 2 mL), CH_3OH (2 x 2 mL) and Et_2O (4 x 2 mL) to afford compound **5** (29.8 mg, 40%) as a yellow solid. Mp: 263 °C (dec).

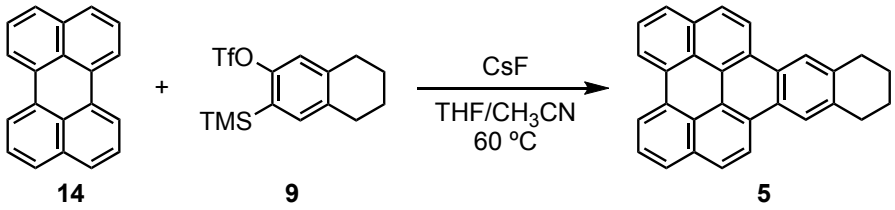

Figure S21. Synthesis of CHNP, **5**.

Spectroscopic data for compound **5**

^{1}H NMR (323 K, 500 MHz, CDCl3), δ: 8.89 (d, J = 9.0 Hz, 2H), 8.83 (d, J = 7.7 Hz, 2H), 8.72 (s, 2H), 8.12 (dd, J = 12.5, 8.5 Hz, 4H), 7.89 (t, J = 7.6 Hz, 2H), 3.24 – 3.21 (m, 4H), 2.06 – 2.02 (m, 4H) ppm. ^{13}C NMR (323 K, 125 MHz, $CDCl_3$), δ: 136.96 (2C), 132.79 (2C), 131.16 (2C), 127.67 (2CH), 127.24 (2C), 127.16 (2C), 127.06 (2CH), 126.43 (2C), 126.29 (2CH), 123.42 (2C), 123.24 (2CH), 122.36 (2CH), 120.72 (2CH), 30.40 (2 CH_2), 23.77 (2 CH_2) ppm. MS (EI), m/z (%): 380.5 (M^+, 100). MS (EI), m/z (%): 380.5 (M^+, 100). HRMS (EI), $C_{30}H_{20}$, calculated: 380.1565, found: 380.1564.

For experimental UV/Vis fluorescence spectra of compound **5** see Fig. S22b. ^{1}H and ^{13}C NMR spectra of compound **5** are shown in Fig. S28.

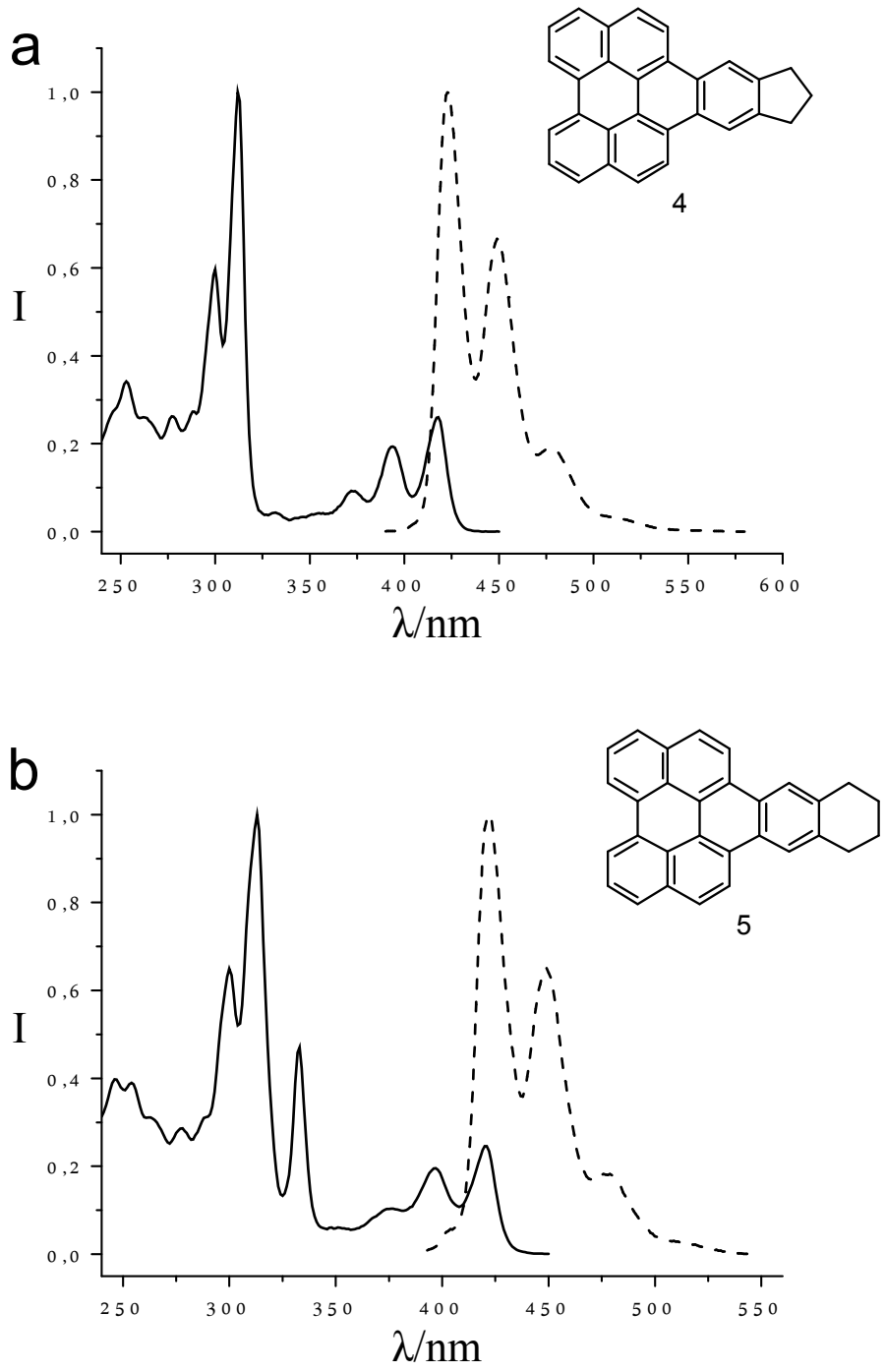

Figure S22. **a** Absorption (solid line) and emission (dashed line) spectra of compound **4** in CH_2Cl_2. **b** Absorption (solid line) and emission (dashed line) spectra of compound **5** in CH_2Cl_2.

11

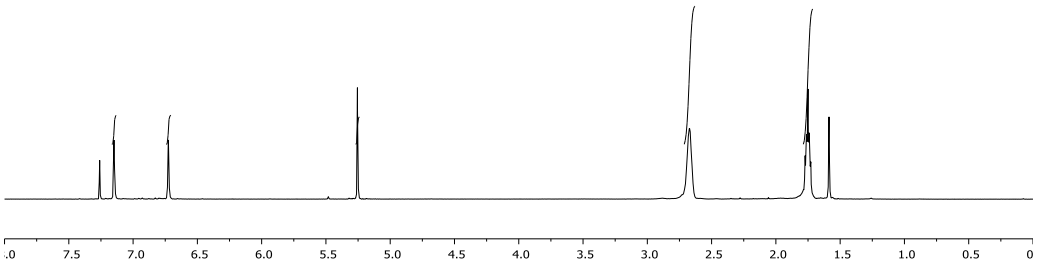

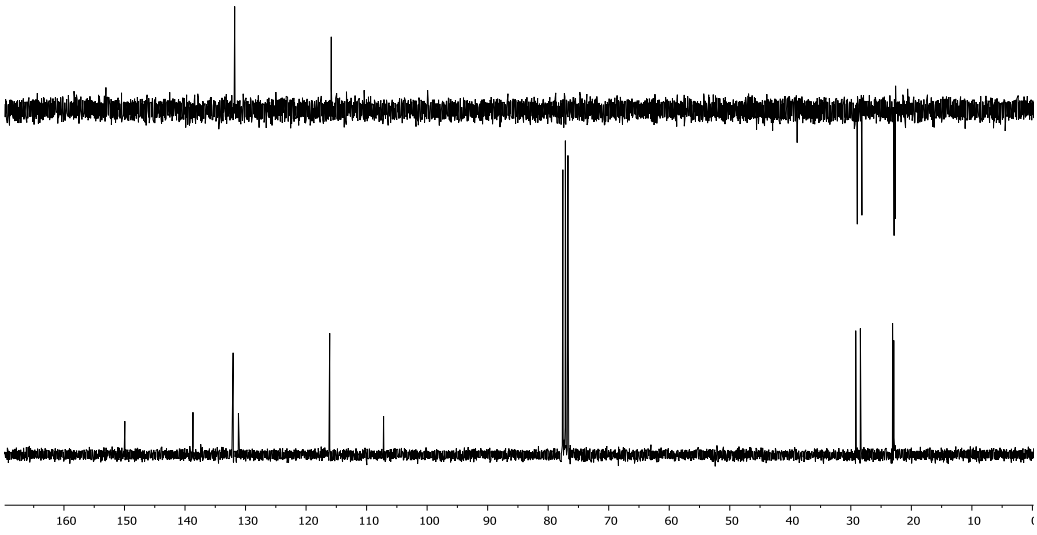

Figure S23. ^{1}H and ^{13}C NMR spectra of **11**.

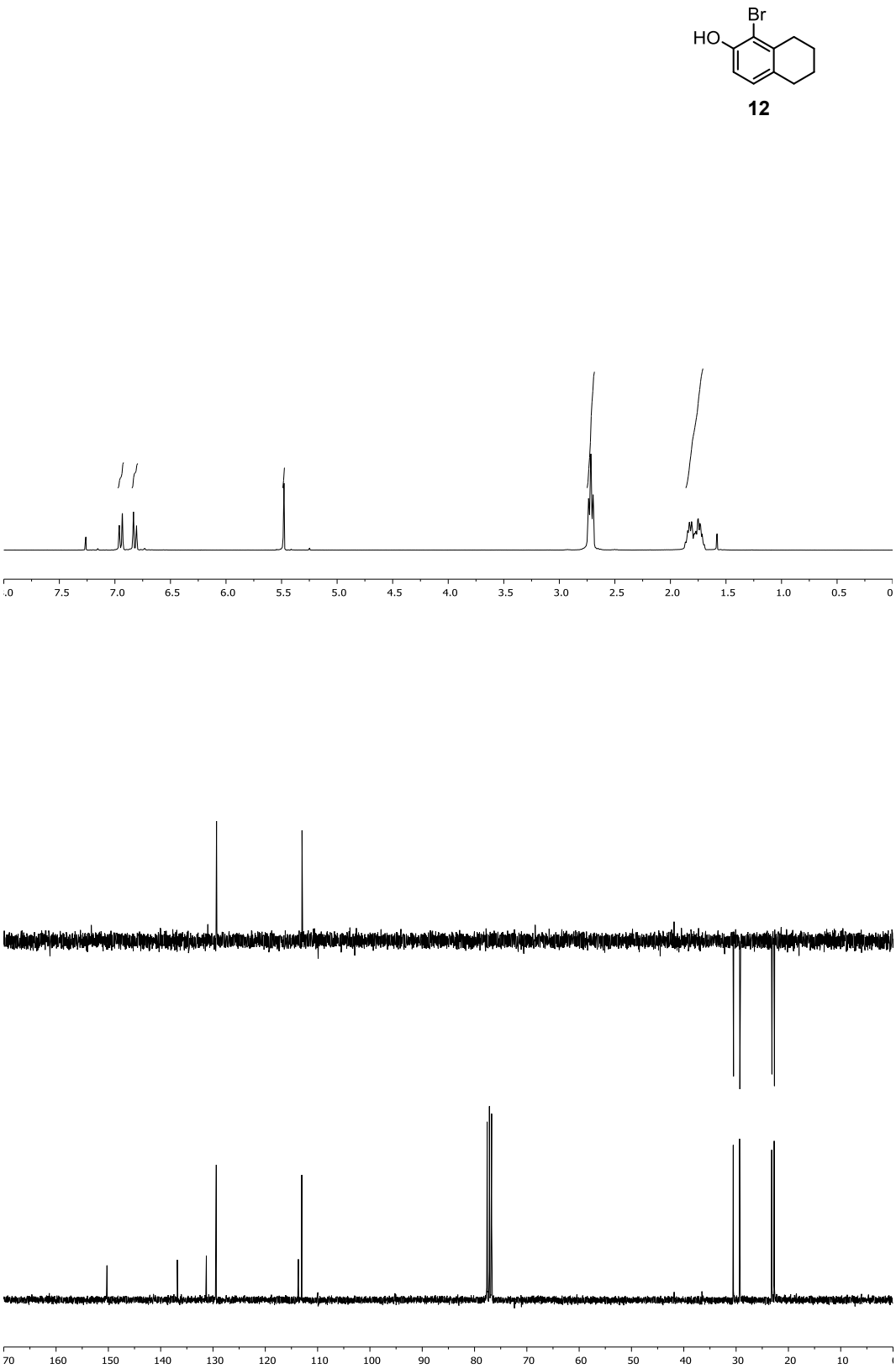

Figure S24. ^{1}H and ^{13}C NMR spectra of **12** .

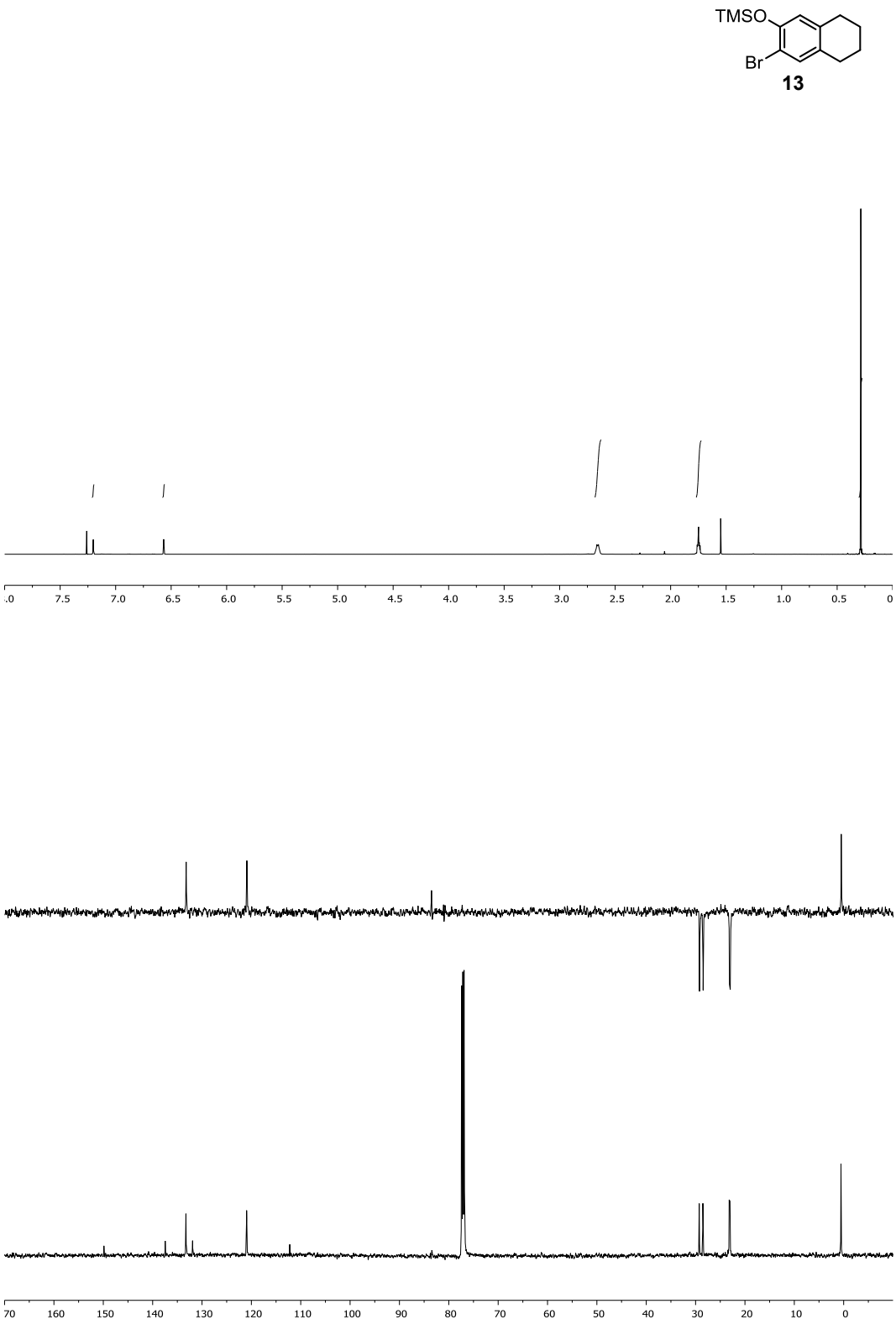

Figure S25. ^{1}H and ^{13}C NMR spectra of **13**.

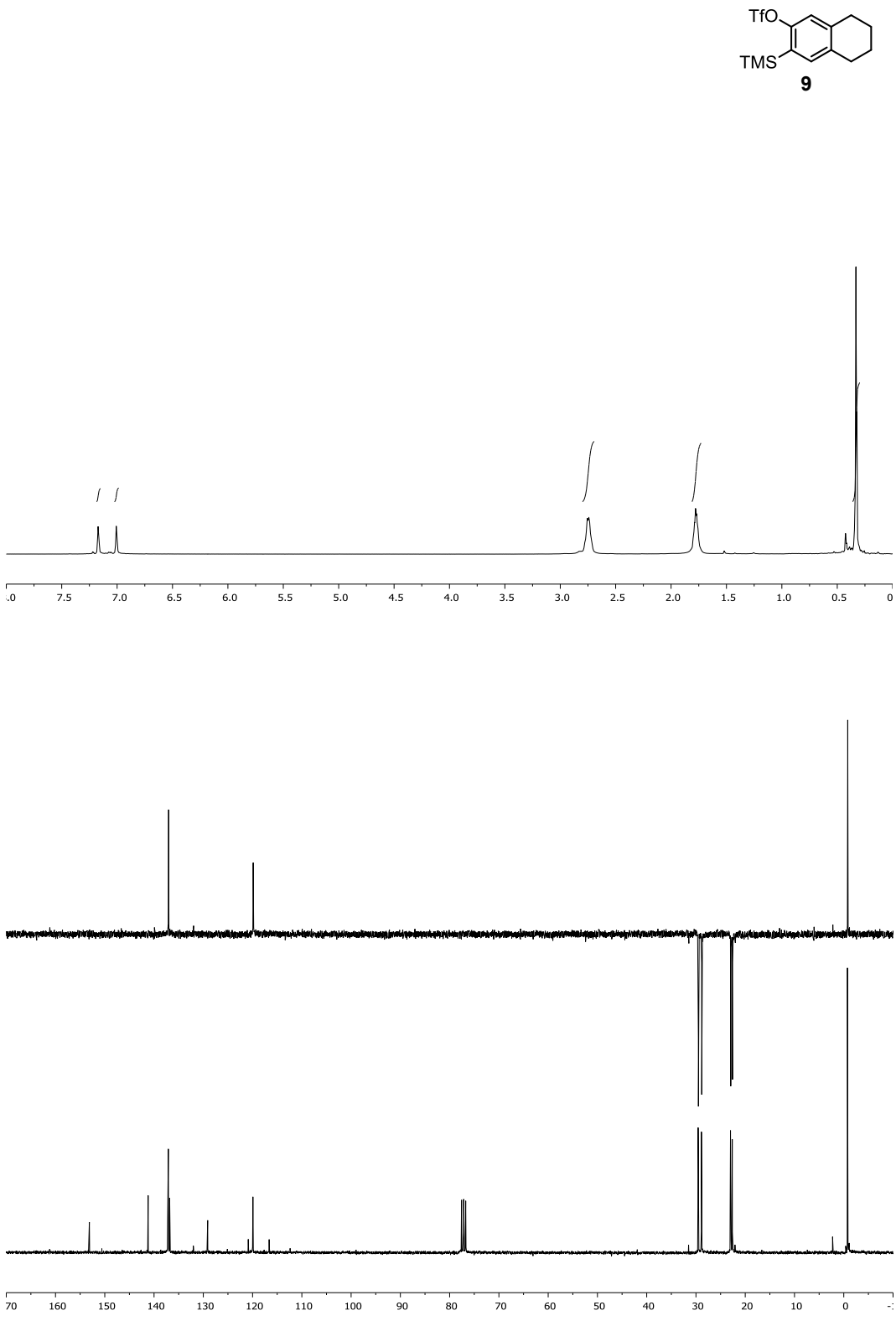

Figure S26. ^{1}H and ^{13}C NMR spectra of **9**.

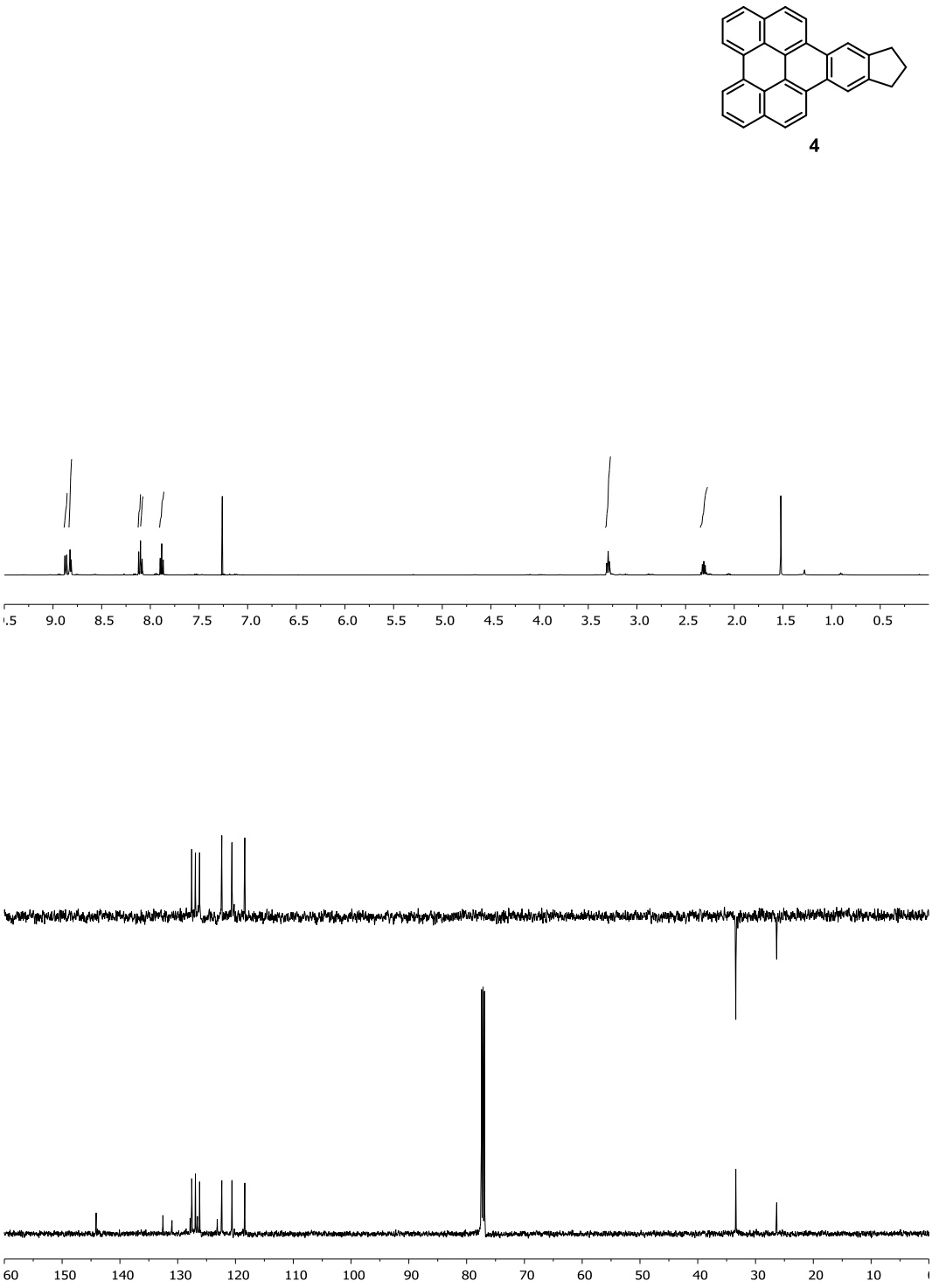

Figure S27. ^{1}H and ^{13}C NMR spectra of CPNP, **4**.

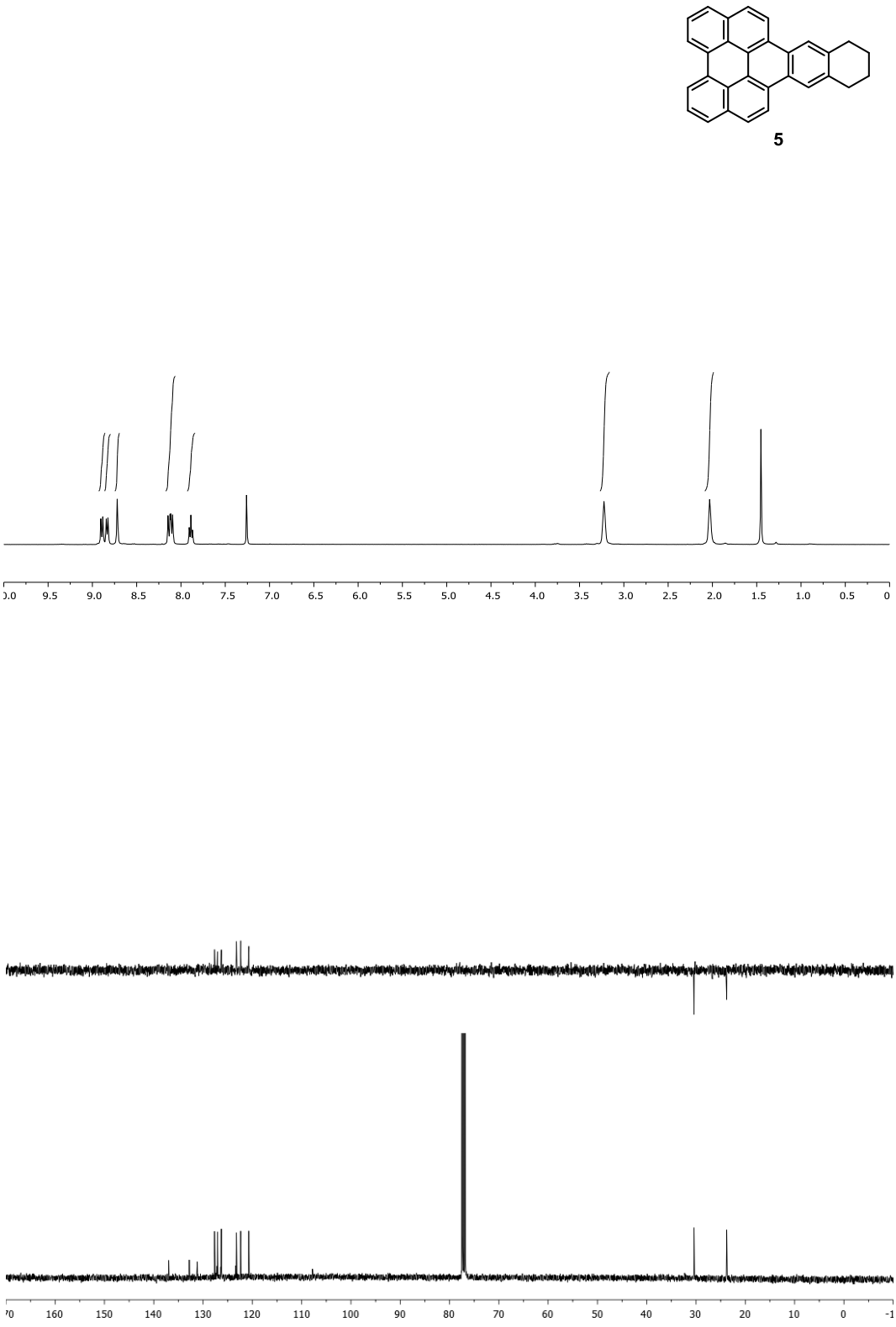

Figure S28. ^{1}H and ^{13}C NMR spectra of CHNP, **5**.

[1] P. Hapala, G. Kichin, C. Wagner, F. S. Tautz, R. Temirov and P. Jelinek, *Phys. Rev. B*, 2014, **90**, 085421.

[2] P. Hapala, R. Temirov, F. S. Tautz and P. Jelínek, *Phys. Rev. Lett.*, 2014, **113**, 226101.

[3] A. J. Weymouth, T. Hofmann and F. J. Giessibl, *Science*, 2014, **343**, 1120–1122.

[4] V. Blum, R. Gehrke, F. Hanke, P. Havu, V. Havu, X. Ren, K. Reuter and M. Scheffler, *Comput. Phys. Commun.*, 2009, **180**, 2175–2196.

[5] B. Schuler, W. Liu, A. Tkatchenko, N. Moll, G. Meyer, A. Mistry, D. Fox and L. Gross, *Phys. Rev. Lett.*, 2013, **111**, 106103.

[6] L. Gross, F. Mohn, N. Moll, B. Schuler, A. Criado, E. Guitián, D. Peña, A. Gourdon and G. Meyer, *Science*, 2012, **337**, 1326–1329.

[7] N. Moll, B. Schuler, S. Kawai, F. Xu, L. Peng, A. Orita, J. Otera, A. Curioni, M. Neu, J. Repp, G. Meyer and L. Gross, *Nano Lett.*, 2014, **14**, 6127–6131.

[8] J. Repp, G. Meyer, S. Stojković, A. Gourdon and C. Joachim, *Phys. Rev. Lett.*, 2005, **94**, 026803.

[9] Y. Kim, T. Komeda and M. Kawai, *Phys. Rev. Lett.*, 2002, **89**, 126104.

[10] P. Reynders, W. Kuehnle and K. A. Zachariasse, *J. Am. Chem. Soc.*, 1990, **112**, 3929–3939.

[11] H. Freund, M. Matturro, W. Olmstead, R. Reynolds and T. Upton, *Energy Fuels*, 1991, **5**, 840–846.

[12] W. Chen, N. B. Zuckerman, J. W. Lewis, J. P. Konopelski and S. Chen, *J. Phys. Chem. C*, 2009, **113**, 16988–16995.

[13] M.-A. Tehfe, F. Dumur, E. Contal, B. Graff, F. Morlet-Savary, D. Gigmes, J.-P. Fouassier and J. Lalevée, *Polym. Chem.*, 2013, **4**, 1625–1634.

[14] I. Quintana, A. J. Boersma, D. Peña, D. Pérez and E. Guitián, *Org. Lett.*, 2006, **8**, 3347–3349.

[15] J. Zhang, X. Chang, E. C. Bowman, C. J. Holt, M. W. Lodewyk, R. M. Miller and G. Xia, *J. Org. Chem.*, 2015, **80**, 9292–9296.